Journal of Engineering and Sustainable Development
https://jeasd.uomustansiriyah.edu.iq/index.php/jeasd
https://doi.org/10.31272/jeasd.28.1.2

Vol. 28, No. 01, January 2024
ISSN 2520-0917

Original Research

IMPACT OF MEASUREMENTS TECHNIQUES ON HEAT TRANSFER CHARACTERISTICS IN AIR JET ARRAYS

Assim Hameed Yousif Al Daraje[1], Afrah Turki Awad[2*], Mohamed Gogazeh[3], Hanan Afeef Mohammad Khamees[4]

[1,3,4] *Department of Mechanical Engineering, Philadelphia University, Amman, Jordon*
[2]*College of Oil and Gas Techniques Engineering - Kirkuk, Northern Technical University, Iraq*
[1]https://orcid.org/0009-0005-1743-4635
[2] https://orcid.org/0000-0003-3967-0821
[3]https://orcid.org/0009-0002-3485-1607
[4]https://orcid.org/0009-0008-7744-1097

Received 18/07/2023 ***Revised 16/10/2023*** ***Accepted 11/11/2023***

Abstract: Air impact processes have diverse applications in engineering, including backflow welding, textile drying, and gas turbine blade and combustion liner cooling. This research examines the influence of experimental methodologies and measurement tools on convective heat transfer in adjustable air jet assemblies. The experiment involves the use of heated targets made of thin stainless steel foil with constant heat flux boundary conditions. Thermography measures target surface temperatures by analyzing how internal passage cross-flow affects convective heat transfer via outflow adjustments. The experiments involve two arrays of jet nozzles: inline and staggering, each comprising 44 impingement jet nozzles arranged in 4 rows with 11 jet holes in each row. The study presents unsteady time average local and spatial Nusselt numbers as functions of jet Reynolds number (4630-14000) and explores their dependence on the jet nozzle diameter. Cross-flow levels significantly affect spatial and local Nusselt numbers in both local and span-wise averaged values, regardless of the Reynolds number. Strong cross-flow (single configuration) distributes flow causing turbulence and uneven heat distribution, reducing Nusselt numbers. In contrast, moderate cross-flow (double configuration) improves heat transfer and increases Nusselt numbers. The study emphasizes the crucial role of experimental techniques in heat transfer evaluation and demonstrates agreement with prior studies within a standard error below 5%.

Keywords: *Air jet flow; impingement cooling; IR cameras; liquid crystal (TLC) technique; local Nusselt number; overall Nusselt number*

1. Introduction

Previous studies primarily focused on the heat transfer characteristics of cooling systems for turbine blades and combustion liners. They aimed to address the challenge of achieving desired temperatures in the combustion chamber and high turbine inlet temperatures [1]. The existing literature extensively investigated factors affecting the thermal performance of impingement systems; including jet Reynolds numbers, geometry, hole arrangement, cross flow, and the spacing between jets. Among these factors, cross-flow has been identified as a key element influencing the cooling characteristics of the impingement process [1].

Previous researchers have extensively studied impingement heat transfers on Perspex flat surfaces or low conductive materials using single and multiple jets and provided valuable insights for designing optimal impingement cooling systems [2]. These studies have investigated parameters including jet impingement angles, distances, height ratios,

*Corresponding Author: afrah.turki@ntu.edu.iq

and geometries, with the heat transfer rate being significantly affected by jet geometry, outlet configuration, and flow variables such as the Reynolds jet number. A reduced spatial Nusselt number occurs when the impingement angle is less than 90°, normal direction [3]. Previous studies by researchers including Zuckerman and Lior, 2005, [4]; San and Lai, 2001, [5]; Changmin et. al., 2001, [6]; Brevet et. al., 2002, [7]; Lamyaa, and Deborah, 2005, [8]; Uysal et. al. 2006, [9]; Yamane1 et. al., 2012, [10]; Shariatmadar, et. al., 2016. [11], have investigated jet geometries. Literature [4-11] has highlighted the benefits of using multiple nozzles to enhance impingement cooling efficiency and achieve uniform heat transfer. Cylindrical holes are commonly used for the jet nozzles, with optimal non-dimensional spacing at x/D = 3 to 4 and y/D = 3 to 4. Previous works have highlighted that heat transfers through the impact of multiple jets are influenced by variables including jet arrangement, nozzle diameter, distance to the target surface, nozzle shape, jet spacing, and Reynolds number. The use of empirical and 'trial and error techniques, supported by experimental and numerical studies, provides reliable and scientifically validated insights [12].

The impact of jet arrangement on flow characteristics and heat transfer has been explored through experimental and numerical investigations, comparing inline and staggered configurations [13]. The experimental model employed circular jets perpendicular to the target surface, revealing a more pronounced influence of cross-flow on the impinging jet in staggered arrangements compared to inline setups. The impact of cross-flow on flow characteristics and heat transfer from impinging jets at low jet-to-plate distances is considered by Wae-hayee et. al., 2014, [14]. Wae-hayee et. al., 2014, [14] employed temporary liquid crystal thermography, which offers detailed temperature measurements on most target surfaces but without time dependence. Results revealed an increase in the peak of the time-averaged local Nusselt number with higher cross-flow rates and a downstream shift in the peak of the Nusselt number. Infrared thermography techniques (Fluke Ti32 camera) were used experimentally to examine heat transfer and pressure loss characteristics in impingement systems [15]. The camera captured a single image without providing time-dependent temperature variations. The evaluation did not account for internal heat loss due to natural radiation and convection, assuming complete removal of heat flux by impingement jets. The testing model included inline round jet holes and staggered arrays with moderate cross-flow rates and a single exit setting. Empirical correlations were derived to predict the spatial Nusselt number based on jet settings parameters for both inline and staggered jet array configurations.

An advanced experimental technique was introduced for jet impingement cooling providing a reliable method to analyze the performance of cooling systems [16]. The experimental setup consisted of an inline multi-hole array with 55 impingement jets under constant heat flux boundary conditions [16]. The results demonstrated an increase in the average time of the local Nusselt number with higher jet Reynolds numbers, both locally and spanwise. Similarly, a study on convective heat transfer was conducted on a 55 impingement jet (5 × 11) setup with constant heat flux boundary conditions [17]. In both of these previous studies, the outflows were directed to include single and double exit configurations. The main objective of Yang et. al., 2022, [18] was to

enhance jet impingement heat transfer under strong cross-flow conditions. Yang et. al., 2022, [18] extended jet holes into the impingement channel, varying the extension length based on cross-flow strength. Experimental measurements used the transient liquid crystal (TLC) technique for jet Reynolds numbers ranging from 1.0 × 104 to 3.0 × 104. The study revealed that the extended jet hole configuration achieved over 10% higher heat transfer compared to the traditional baseline configuration, with the same pumping power. An investigation of heat transfer is conducted between circular jet arrays and a moving surface, considering both inline and staggered jet patterns, revealing significant effects on surface motion and jet cooling patterns [19]. On the other hand, a numerical study was conducted to examine the effects of varying jet diameters on the cooling efficiency of single-row jet impingement in a semicircular target channel with a single exit [20]. The study aimed to mitigate cross-flow effects through different jet diameter arrangements and Reynolds numbers. The research established the relationship between the mass velocity ratio and jet hole area, highlighted vertical structures, and discussed the distribution of Nusselt numbers. The findings revealed that optimizing the jet diameter arrangement reduces non-uniformity in peak Nusselt numbers.

Furthermore, the impact of impinging air jet movement on fixed flat plate heat transfer was studied by varying nozzle velocity (Vn) and Reynolds number (Re) within specific parameters [21]. The results demonstrated a peak local Nusselt number at Vn of 400 mm/min, Re of 20,000, and H/D of 2, accompanied by enhanced heat transfer uniformity and sustained higher values at Vn of 1000 mm/min, Re of 20,000, and H/D of 6.

The impact of extended jet holes on heat transfer in an in-line array jet impingement configuration on a flat surface has been investigated through experimental and numerical methods, revealing optimized conditions for enhanced heat transfer performance across various parameters such as jet spacing, plate-to-plate distance, and nozzle-to-target plate gap [22]. An experimental study explored the improved thermal performance of novel finned copper foam heat sinks exposed to jet impingement cooling for electronic devices, showcasing their capability to surpass conventional finned heat sinks, albeit with increased pressure drops [23]. It was observed that the performance of inline jet array configuration exhibited a marginally superior outcome when compared to staggered arrangements [24]. On the other hand, a statistical analysis was utilized to assess numerical predictions of temperature distribution for two categories of heat sinks featuring impingement arrays: flat plate heat sinks and arc-fins heat sinks (Models A, B, C, D, and E) [25]. The findings highlight the superior efficiency of arc-fin heat sinks, especially Model D, showcasing the positive influence of a concave arc positioned near the heat sink's exit. This influence was supported by a reduction of 12% and 8% in the average heat sink temperature at Re (7000, 9000), respectively, and a consistent enhancement of 8% and 7% at Re (11000), as compared to the flat plate heat sink. The correlation coefficients varied across the different models.

Moreover, it was discovered that increasing the stream-wise jet-to-jet spacing or decreasing the jet hole-to-target plate distance enhances the performance by reducing thermal resistance and improving temperature uniformity [26].

Smaller nozzle-to-plate distances generally lead to better performance compared to cases with larger distances in the same apparatus [27]. According to the literature, it is important to investigate the effects of experimental facilities and test techniques on evaluating the heat transfer performance of jet-impinging arrays. This paper provides experimental investigations that contribute to:

1. A broader understanding of convective heat transfer characteristics and the minimization of complexities and limitations in understanding impingement mechanisms.
2. Recognizing the cross-flow phenomenon improves impingement cooling performance.
3. Consideration of methodological and experimental techniques is essential alongside infrared thermography for cooling analysis.
4. Inline and staggered jet settings with round multi-hole arrays and fixed low jet-to-plate distances illustrate the jet-cross flow interaction.
5. Variations in Jet Reynolds number and single/double settings are considered.
6. Array impingement jets involve convection through advection and diffusion, enhancing the understanding of fluid dynamics in this study.

2. Experimental Set-Up and Methodology

The experimental facility is equipped with electrically heated stainless steel foil, which is cooled by incorporating a jet array. The heated foil maintains a constant temperature on one side using a controller to sustain a constant temperature without significant fluctuations and is insulated on the other. As a result, the foil enables infrared cameras to capture images of the side opposite to the impingement.

2.1. Test Rig

The test rig is supplied with air from a 1.1 kW pressure air blower, ensuring a flow rate of 140 m^3/hr at 175 kPa. The mass flow rate is measured using a standard orifice flow meter with an orifice diameter of 26.5mm, which is 0.53 times the diameter of the pipe. The pressure difference is measured using a digital manometer. To ensure a uniform flow through the orifice meter, a thin cross-fin straightener is mounted upstream of the orifice plate in the piping system. The airflow passes through contractions, transitioning through the pipe to the settling chamber and upper plenum before reaching the test section. The settling chamber utilizes diffusing meshes for uniform airflow, while the Aluminium sheets primarily construct the settling chamber and upper plenum. The settling chamber and upper plenum are made primarily of 2mm thick Aluminium sheets. The transparent acrylic walls enclose the remaining test section, which comprises a perforated plate (impingement jet nozzles), lower plenum (60 mm x 200 mm), adjustable spacer for jet distance, and a heated foil target surface. The test section also includes two closable exits when needed. Fig. 1. illustrates the schematic layout of the test rig and the experimental setup.

The air, after passing through the nozzle plate and impacting the impingement surface, is discharged through single or double exits maintained at atmospheric pressure. In the single exit configuration, the jet air is forced to exhaust in one direction, resulting in increased cross flow.

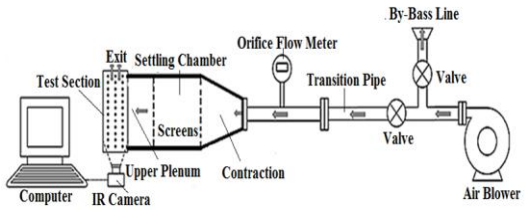

a. Schematic Layout of the Test Rig

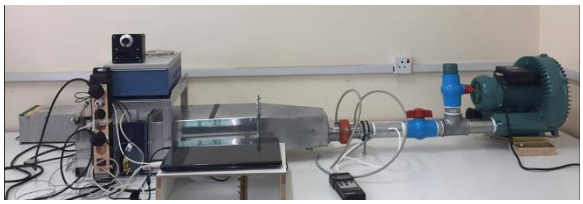

b. Test Rig

Figure 1. a. Schematic Layout of the Test Rig and b. the Test Rig.

The perforated plate (200mm x 300mm) contains four rows of discharge jet nozzles, with both inline and staggered jet settings having the same jet number of 4 lines, each row consisting of 11 nozzles, resulting in a rectangular group of 44 jets. The attachment jet nozzle array is centrally positioned on the perforated plate. A transparent Acrylic spacing frame (60mm x 200mm) separates the nozzle exit from the target foil. Each impingement jet nozzle is a cylindrical hole drilled into the nozzle plate with a diameter (D) of 5mm. Both settings have the same sidewall distance, utilizing the dimensions of the upper plenum. The non-dimensional distance between adjacent holes in the x and y directions for both models is X=x/D = 3 and Y=y/D = 3. The nozzle exit-to-foil target distance is set at H = 3D. The nozzle plate consists of a thick 3D Aluminium plate. The air supply follows a joint flow arrangement. Fig. 2 shows the scheme of setting a jet array arrangement (all dimensions in mm). Table 1 shows the differences between inline and staggered arrangements.

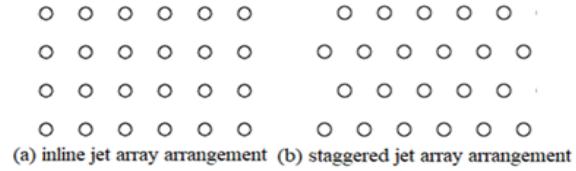

Figure 2. Jet Array Arrangements (all dimensions in mm)

Table 1. The differences between inline and staggered arrangements.

Aspect	Inline Array	Staggered Array
Arrangement	Jets aligned in a single row	Jets staggered in offset rows
Flow Pattern	More organized and predictable	Turbulent
Obstruction	Potential obstruction between adjacent jets	Reduced obstruction between jets
Cross Flow	Moderate cross flow	Strong cross flow
Heat Transfer	Even heat distribution	Uneven heat distribution

After passing through the nozzle plate and impacting the surface, the air is discharged through either a single or double exit configuration, both maintained at atmospheric pressure. In the single exit setting, the jet air is directed in one direction, leading to an increased cross-flow. Fig. 3 shows a cross-sectional view of the settling chamber and the test section.

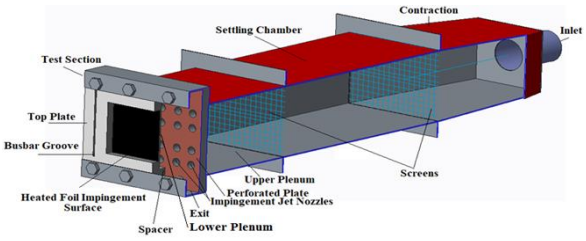

Figure 3. Cross-Sectional View of the Settling Chamber and the Test Section

The test sequence begins by activating the air blower and adjusting the air mass flow rate using passing and bypass valves to achieve the desired Reynolds number. Once the DC power

supply is turned on, the temperature of the heated foil is controlled by adjusting the DC supply. When the maximum temperature stabilizes to around 75°C, the IR camera is brought online. After ensuring the stability of all test functions, the IR camera records a 10-second video sequence, resulting in 1,200 frames for each test.

2.2. Heated Target and Power Supply

Thin stainless steel foil (304, I.S. 04Cr18Ni10) with a thickness of approximately 40 µm is used as the heated target surface. The foil's thickness is measured using a digital thickness gauge during the assembly process. It is volumetrically heated through Joule heating and placed on the inside of a 15 mm thick Acrylic top plate. Rectangular openings (60mm x 200mm) are cut on the Acrylic upper plate, allowing imaging of the opposite side of the foil. The foil is securely attached to a thick set of pure copper bus bars, ensuring tightness and flatness during assembly to maintain a flat and smooth foil surface. This prevents any impact from the stagnation pressure of the impingement jet and thermal expansion due to temperature rise. The copper bus bars are embedded in grooves worked into the Acrylic top plate. Fig. 4 depicts the dimensions of the Acrylic Top Plate, with all measurements in millimeters (mm).

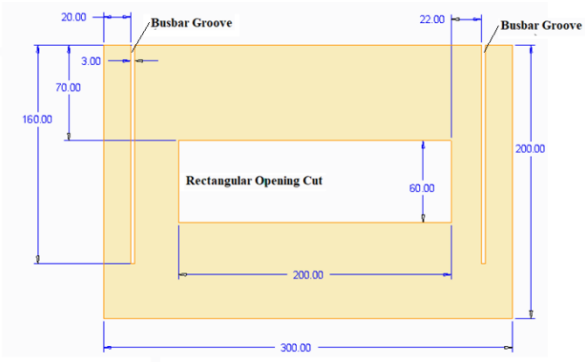

Figure 4. Acrylic Top Plate Dimensions, all dimensions are in (mm)

The foil is heated to a specific temperature using a controlled DC electric current supplied through a digital design system. The volumetric resistance of the stainless steel varies based on the alloy type and temperature. The tension applied to the foil ensures a flat and smooth target surface. The heat flux is determined by measuring the voltage and electric current that passes through the foil.

The foil is heated using a digitally controlled power supply system developed by [28]. The voltage drop across the foil is measured to determine the potential difference between two terminal points. Two 0.25 mm copper cables are soldered at each terminal point, with a distance (l) of 6 cm between them. LAH 100-P current sensors manufactured by LEM USA Inc. are used to measure the DC electrical current. To validate the measurement of surface temperature obtained through an IR camera, two type K thermocouples are placed in separate locations to measure the foil's surface temperature. The power supply ensures a stable voltage below 3 volts during testing. The temperature of the foil ranges from the normal room temperature to 150°C. To achieve specific temperature changes of 0.5°C increments, precise adjustments in both current and voltage readings are made. The system display digitally shows the voltage drops, current drawn, and temperature.

2.3. Experiments Procedure and Methodology

Based on the conducted experiments and the disparities between test conditions and actual machine conditions in previous experiments, dimensionless parameters were utilized to measure the results. The impingement jet is characterized by the jet Reynolds number, while heat transfer is characterized by the Nusselt number. Four different impingement jet Reynolds numbers (Re_j) were established. To

maintain a constant heat flux through the foil, convective cooling is achieved using a continuous flow of air jets. The nozzle mass flow rate is determined based on the measured average flow rate and air density at the nozzle. The total mass flow rate and jet velocity through the 44 impingement jet nozzles (n) are measured accordingly. The average mass flow rate for each impingement jet nozzle is calculated by considering the weighted area. The Reynolds number for flow through each jet nozzle is determined individually using the following Equation (1).

$$Re_j = \frac{VD}{v} \quad (1)$$

Where v is the jet velocity (m/s), ν is kinematic fluid viscosity (m^2/s), and is estimated using the Sutherland Equation and D is the diameter of the jet nozzle (m). The jet Mach number (M) represents the dimensionless velocity and is defined by Equation (2).

$$M = \frac{V}{a} \quad (2)$$

The local sound speed (a m/s) is measured in the impingement jet nozzle, with the Mach number ranging from 0.135 to 0.7 for all cases. The fluid temperature inside the jet nozzle is assumed to be the same as the temperature in the upper plenum. Due to the low Mach number, the difference between static temperature and total temperature is negligible and can be disregarded.

2.4. Surface Temperature Measurements

Thermocouple techniques provide data at various locations on the foil surface and validate IR camera temperature readings. Surface temperature measurements are obtained using IR cameras (PCE-P1160) equipped with BI-SPECTRAL technology. The camera has a resolution of 160 x 120 pixels and a USB 2.0 interface, enabling real-time imaging at 120 frames per second. The foil surface is coated with a very thin layer of black paint (<1 μm) with high thermal conductivity, ensuring negligible additional thermal conduction. The emissivity of the black surface is determined using the measurement procedures of Ou and Rivir [29], yielding similar results to previous experiences. As both sides of the foil are assumed to have the same temperature distribution, the IR camera captures the spatial temperature distribution ($T_{s(x,y,t)}$) on the foil surface affected by the jet. The surface temperature data from each frame is converted to MATLAB data file format for further processing.

The measurement domain is configured using the PI Connect software, with care taken to avoid additional thermal conduction near the bus bar connection by selecting a measurement distance of 1.25 cm from each bus bar. During testing, the measurement domain is adjusted to view only 40 impingement jets, resulting in an image resolution of approximately 2.06 pixels/mm2 or 0.48 mm^2/pixel. The fluid temperature in the upper plenum is measured using three K-T type thermocouple plugs, with temperature data recorded on the computer. The temperature differences in the upper plenum remain within 2°C across all cases. The IR camera records video sequences and detailed frames during the experiment for further analysis and documentation using Vista window 10. Data analysis is performed offline when the IR camera is disconnected. Radiometric snapshots are cropped and stored in radiometric files, while real-time temperature information is displayed digitally or graphically. Temperature and analysis data are stored in Excel text files. Real-time data transfer includes the average temperature of the upper plenum and the local target temperature, which are collected and

transferred to the MATLAB software application. Numerical processing of the results is performed for each case based on the Reynolds jet number and heat flux. The analysis is supported by the measurement of hot and cold points in the captured images.

3. Convective Heat Transfer Parameters Evaluations

The thin foil has a uniform thickness, providing approximately 98% uniformity and allowing for a nearly uniform heat flux. The jet cooling characteristic enhances heat transfer near the stagnation point but decreases between the jets, resulting in lateral heat conduction within the foil. To minimize lateral heat conduction, a thin foil technique is employed, which is suitable when the heat transfer gradient is low enough to neglect lateral heat conduction. Thus, a 2-dimensional approach can be used to simulate the process. In a steady state, the energy transferred to the heated foil can be described by Equations (3 and 4).

$$\dot{\boldsymbol{q}}_{\boldsymbol{net}} = h_{(x,y,t)} \left(T_{s(x,y,t)} - T_m\right) \quad (3)$$

$$\dot{\boldsymbol{q}}_{\boldsymbol{net}} = \left(\dot{q}_{foil} - \dot{q}_{losses\,(x,y,t)}\right) \quad (4)$$

The heat flux ($\dot{\boldsymbol{q}}_{\boldsymbol{foil}}$, W/m^2) on the heated foil surface can be determined based on the voltage drop across the foil and the current passing through it. The heat flux is represented by Equation (5).

$$\dot{q}_{foil} = \frac{I\,V}{l\,w} \quad (5)$$

Where (I) is the current passing through the foil (Amps), (V) is the voltage drop across the foil heater between two attachment points (Volts), (l) is the distance between the two attachment points (m), and (w) the foil width (m).

The local convective heat transfer coefficient ($h_{(x,y,t)}$, W/m^2 K) on the target surface is determined using equation (3). This coefficient is non-dimensional, relating $h_{(x,y,t)}$, to the jet hole diameter D and the local thermal conductivity ($k_{(x,y,t)}$, W/m. K) based on the film temperature ($T_{film\,(x,y,t)}$, ^{0}C) of the fluid. The non-dimensional heat transfer coefficient can be calculated using equation (6), which defines the local Nusselt Number as the average local time Nusselt number ($\overline{Nu}_{(x,y,t)}$) based on the jet hole diameter D.

$$\overline{Nu}_{(x,y,t)} = \frac{(h_{(x,y,t)})\,\mathrm{D}}{k_{(x,y,t)}} \quad (6)$$

$$T_{film\,(x,y,t)} = \frac{T_{s\,(x,y,t)} + T_m}{2} \quad (7)$$

The term $\dot{q}_{losses\,(x,y,t)}$ is assessed following the approach by Schroder et al [16] to account for radiation and natural convection losses on the imaged side of the foil. Schroder et al[16] estimated these losses to be approximately 3-4% of the total heat produced by the foil heaters, considering radiation losses based on Stefan-Boltzmann's law for local surface temperatures ($T_{s\,(x,y,t)}$). As a result, the foil heaters behave as nearly isothermal surfaces locally, with forced convection from jet impingement being the dominant factor affecting the temperature. The estimation of natural convection heat loss by Schroder et al. [16] is based on the correlation for laminar-free convection of isothermal vertical surfaces, initially introduced by Bejan [30]. Thus, the combined radiation and natural convection losses amount to approximately 7% of the total heat produced by the foil heater($\dot{q}_{foil}$). Currently, both losses are assumed to be at this level.

4. Uncertainty of Experimental Results

The Kline and McClintock [31] approach for single-sample uncertainty is employed in the current experimental work, with all uncertainties reported at a 95% confidence level. The

absolute uncertainties for the Nusselt number depend on factors such as measuring temperature errors of the working fluid and foil surface, as well as errors associated with measuring heat flux (voltages and current). Similarly, for jet Reynolds numbers, uncertainties arise from measuring the pressure difference across the orifice plate, the temperature of the working fluid upstream of the orifice entrance, and determining the working fluid temperature. Kline & McClintock [31] provided a method for combining the effects of multiple errors. The jet diameter and heated area of the domain have no associated uncertainty, as they are exactly 5mm and 90x190 mm², respectively. The absolute uncertainties for the Nusselt number are higher at low Reynolds numbers, around ±8%, while the uncertainty for the jet Reynolds number is estimated to be approximately ±2.2%. At high Reynolds numbers, the pressure difference across the orifice and the foil heat flux significantly increase, resulting in lower uncertainties for both the Nusselt number and Reynolds number. The uncertainty in measuring surface temperature using thermography is estimated to be around ±2.0°C.

5. Target Surface Temperature Field

The experiment involved four cases: (1) inline jet array with single exit, (2) inline jet array with double exit, (3) staggered jet array with single exit, and (4) staggered jet array with double exit.

Four thermal image samples illustrating the target domain temperature field for Re_j= 11800 are shown in Fig. 5. These images display the temperature distribution as colored hot and cold spots, clearly indicating the impact of jet array arrangement and cross flow. The colors change according to the temperature variations on the foil target, providing valuable insights into the experimental data quality.

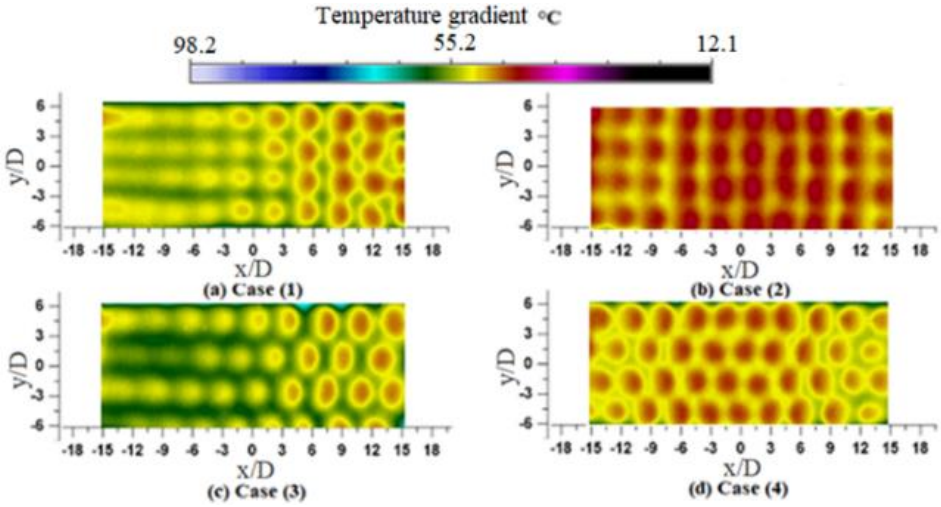

Figure 5. Thermal Images- Surface Target domain temperature field for $Re_j = 11800$

Due to jet-to-jet interactions, the cooling effect gradually decreases downstream, as shown in Fig 6 (a), (b), (c), and (d). In single exit configurations (cases 1 and 3), represented by Fig 6 (a) and (c), the forced flow in one direction results in a stronger cross flow as it approaches the exit, affecting the heat transfer benefits from the jet. Compared to inline jet arrays (images 1 and 2), the cooling effect is relatively higher due to less obstruction between adjacent jet lines in staggered jet arrays. The cross-flow from the previous jet in adjacent rows has a significant impact on the downstream jet in cases 3 and 4. These effects are demonstrated in Fig. 5.

6. Evaluation of the Local Heat Transfer Characteristics

When the jet impinges on the target plate, a divider flow is formed in the direction of the airflow. Viscous forces cause a reduction in velocity and thickening of the divider flow as it moves away from the center. The point of stagnation experiences the highest velocity and provides efficient heat removal, resulting in a high local Nusselt number$(\overline{Nu}_{(x,y,t)})$. As the jet moves towards the exit, its velocity gradually decreases. This leads to a significant reduction in the local Nusselt numbers in the central region surrounding the jet. The interaction between impingement jets and cross-flow enhances the turbulent intensity in the jet core, resulting in the lowest local Nusselt numbers in the central region in both the x and y directions for all cases. It is well-known that the Nusselt number peaks at the stagnation area, where the convective heat transfer coefficient is highest in the middle of the jet stream. The unsteady local Nusselt numbers are estimated along (x/D) using a surface temperature of 19200 pixels per frame. The local Nusselt numbers are determined by averaging the local surface temperatures along the y-axis, specifically the spanwise average surface temperature ($T_{s,spanwise\,(x,t)}$) at different x/D values. Fig. 6 illustrates the distribution of local Nusselt numbers with Re_j. The highest local Nusselt number is observed at the center of the jet impact area for all cases and Reynolds number ranges. This could be due to intense heat transfer caused by high-velocity flow and turbulence [32]. This effective mixing between the jet and surface maximizes heat transfer, creating a consistent pattern across different cases and Reynolds number ranges [32].

Fig 6 demonstrates that double exits surpass single exits and inline configurations outperform staggered ones, these trends are attributed to specific flow patterns. Double exits distribute heat more evenly over a larger area, enhancing mixing and heat transfer. In contrast, single exits concentrate flow in a smaller area, generating higher velocities and turbulence, yet potentially uneven coverage. Similarly, inline arrangements, with their organized flow, ensure sequential and effective heat transfer. Staggered setups, marked by turbulent but less organized flow, can result in uneven heat transfer regions. These patterns consistently hold across various Reynolds numbers, underscoring their effectiveness in maximizing convective heat transfer.

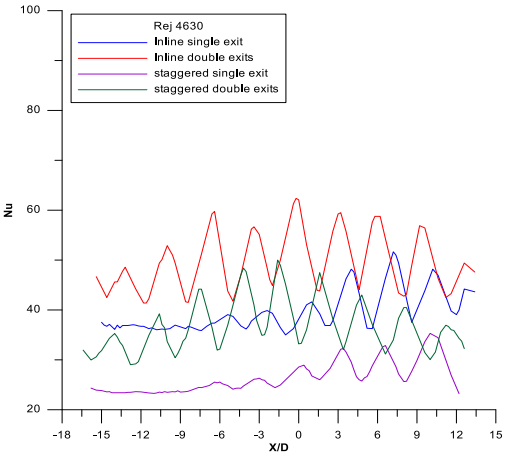

a. Re_j= 4630

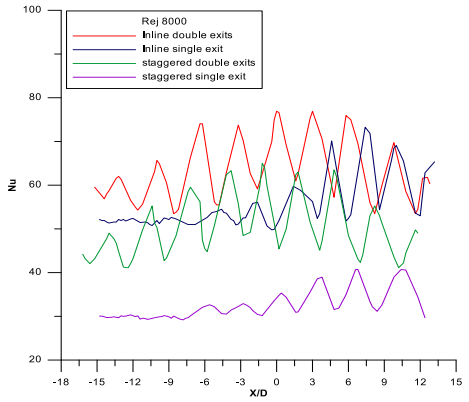

b. Re_j= 8000

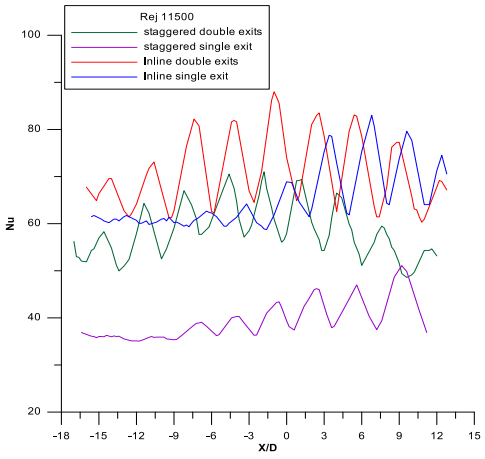

c. Re_j= 11500

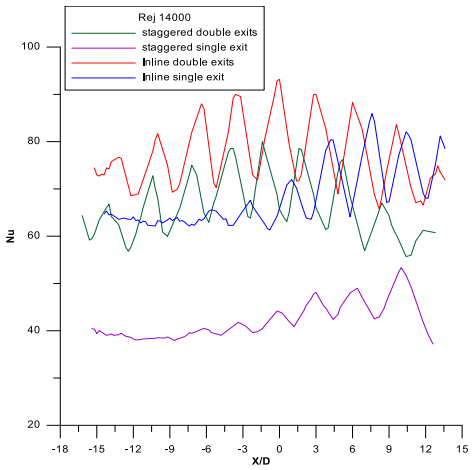

d. Re_j= 14000

Figure 6. The Average Local Nusselt Number Distributions, along the x-axis at different values of Re_j

In Fig. 7, it can be seen that inline cases (1) and (2) have higher local Nusselt numbers compared to staggered cases (3) and (4). The impact area shifts due to strong cross-flow with downstream jets, deviating from the previous jet impact area. The local Nusselt number decreases monotonically downstream for the single exit staggered case, with a peak at x/D = 7.5 and a decrease towards the exit. This behavior is similar to what [16] has observed.

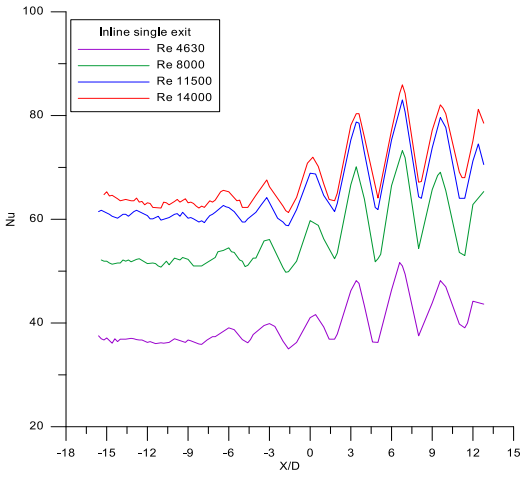

a. Inline single exit at different values of Re_j

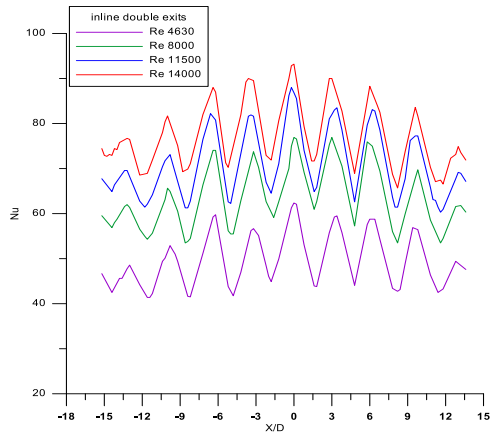

b. Inline double exit at different values of Re_j

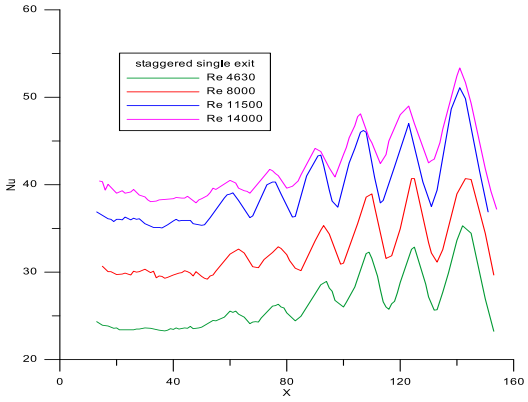

c. staggered single exit at different values of Re_j

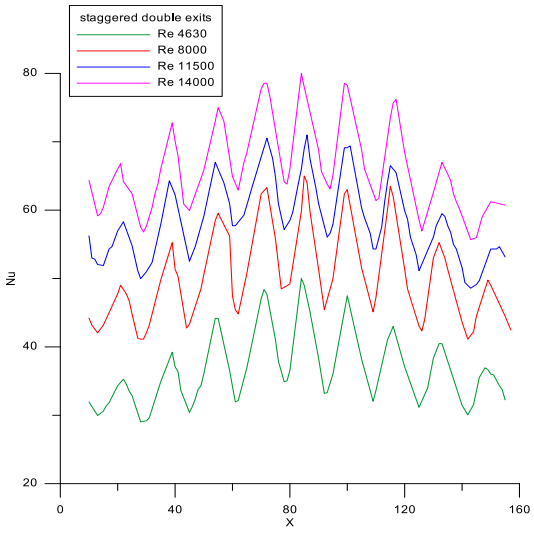

d. staggered double exit at different values of Re_j

Figure 7. Time Average Local Nusselt Number Distributions Along x-axis for All Cases at different values of Re_j

In Fig. 7, the local Nusselt number along the x-direction is shown for all cases at different values of Re_j. In case (1), the peak Nusselt number in each jet impact area increases from x/D = 15 to 6. This is attributed to the development of a strong cross-flow downstream, causing the jet effect area to expand towards the exit. Consequently, the cross-flow intensity gradually increases towards the exit, leading to enhanced local Nusselt numbers. However, between x/D = 6 and -15, the cross-flow intensifies significantly, causing a gradual shift in the Nusselt number peak within the jet's core region due to the lower jet momentum near the surface.

In case (3), the peak local Nusselt number decreases continuously downstream until the exit, influenced by the strong cross-flow originating from adjacent jet rows. In case (1), the local Nusselt number increases from x/D = 15 to 9 and then decreases downstream, reaching its lowest value at the exit. Fig. 7, cases (2 and 4), demonstrate that the maximum local Nusselt number occurs at x/D = 0, and it decreases symmetrically on both sides towards the exit. Similar findings were reported by [16]. The local Nusselt numbers' peaks are influenced by the jet nozzle pattern and flow exit settings. In case 1 and case 3, high local Nusselt numbers are observed at the closed end, while they decrease in the open exit area where the cross-flow is most intense. In the double exit setup (case 2 and case 4), the local Nusselt number is high at x/D = 0, as the cross flow is minimal. Fig. 8 illustrates an increase in the peak local Nusselt number with the increasing cross flow, consistent with the findings of [14].

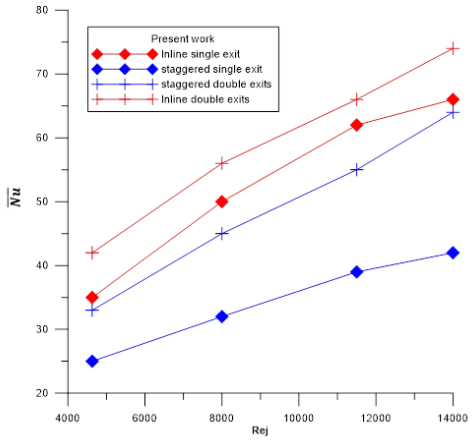

Figure 8. Spatial Time and Area Average Nusselt Number ($\overline{Nu}$) versus Reynolds numbers

The maximum peak value of the local Nusselt number across all cases is 194. In both inline and staggered jet arrays, the cross-flow strength increases towards the exit. The distribution of the local Nusselt number along the x-axis changes from a sinusoidal pattern to a rough line pattern as the flow moves downstream. Moreover, the area with high local Nusselt numbers shifts away from the center line of the nozzle array. This behavior aligns with the findings of [16], indicating that the location of the highest Nusselt number value changes in both the x and y directions as the flow moves towards the exit. These results are consistent with the findings of [16].

7. Evaluation of the Overall Heat Transfer Characteristics

Fig. 8 illustrates the variations in Spatial Time and Area Average Nusselt Number versus ($\overline{Nu}$) versus Reynolds numbers for all cases. The spatial Nusselt number is determined by averaging the temperature across the entire estimated surface. In both inline and staggered arrays, increasing the Reynolds number leads to higher spatial Nusselt numbers. Comparing case 2 to case 3 in the double exit setup, case 2 has higher spatial Nusselt numbers by 36.7%, 34.6%, 29%, and 26.3%. Similarly, in the single exit setup, case 1 has higher spatial Nusselt numbers than case 3 by 36.36%, 36%, 33.8%, and 36.36%. In the double exit setup, case 2 has higher spatial Nusselt numbers than case 4 by 6%, 12.5%, 16.6%, and 16.6%. Notably, in cases with a strong cross-flow (staggered arrangement), the spatial Nusselt numbers are lower than in cases with a moderate cross-flow (inline arrangement) for both exit setups.

Fig. 9 displays the spatial Area Averaged Nusselt number versus Reynolds numbers for inline jet array arrangements, including the findings of previous experimental works by [14-16].

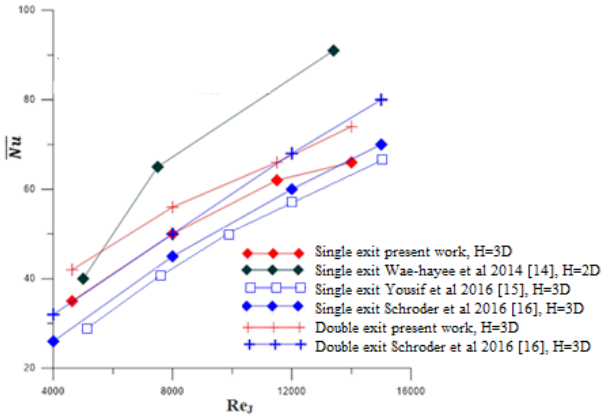

Figure 9. Spatial Area Averaged Nusselt Number versus Reynolds numbers for Inline Jet Array Arrangement

Similarly, Fig. 10 compares the present work with the previous works by [14-15] for staggered jet arrangements. In both figures, the spatial Nusselt numbers exhibit similar behavior, increasing as the Reynolds number (Re_j) increases.

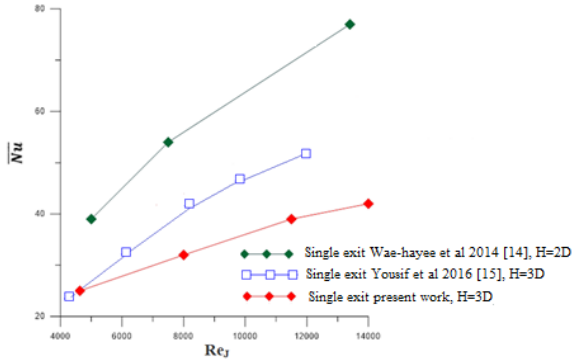

Figure 10. Spatial Area Averaged Nusselt Number versus Reynolds numbers for Staggered Jet Array Arrangement

8. Results Comparability with Previous Work

Comparing the present results of the inline jet array arrangement with [14-16] for the single exit setup, the spatial Nusselt number values are similar to [16], slightly higher at Re_j= 4630, 8000, and 11500, and slightly lower at Re_j= 14000. This agreement can be attributed to the use of the same experimental technique, jet nozzle geometry, jet nozzle arrangement, and thermal boundary conditions. However, there is a discrepancy with the results of [14] who used a transient liquid crystal thermography technique for temperature measurement, which introduces complexity and alignment challenges. Similarly, the results of [15], which analyzed heat transfer characteristics on a flat Perspex surface with low conductivity, do not match the present results. It should be noted that the temperature estimation methods employed by [14-15] do not consider the temporal aspect of temperature on the target surface.

9. Conclusions

In this study, experiments were conducted to observe the unsteady heat transfer characteristics of impingement cooling using inline and staggered jet arrays on a thin heated target. Each array consists of 44 impingement nozzles, and a constant heat flux boundary condition is maintained at the target. Target surface temperature is measured using steady infrared thermography. Strong and moderate cross-flow levels were considered, with single and double exit setups. The results include time-averaged local and spatial Nusselt numbers evaluated at Re_j of 4630, 8000, 11500, and 14000, with a fixed jet spacing of (H/D=3). The cross-flow level for the staggered array is higher compared to the inline array. The presence of moderate cross flow with a double exit setup increases the convective heat transfer values for both jet arrays. The Nusselt number demonstrates a linear correlation with the jet Reynolds number, rising with increased Reynolds numbers in local and spanwise dimensions. Strong cross flow in the single exit setup notably impacts the time-averaged local Nusselt number, regardless of Reynolds numbers. Staggered jet arrays offer superior cooling effects due to reduced obstruction between adjacent jet lines, contrasting with inline arrays.

Additionally, the cross-flow significantly influences the heat transfer/mass characteristics (Sherwood number) of the target plate. It was found that variation of local and overall Nusselt numbers with the jet Reynolds number provides insights into convective heat and mass transfer coefficients. The methodology and experimental techniques play a crucial role in determining the value of convective heat transfer characteristics.

Acknowledgments

This research project was supported by Philadelphia University, the Deanship of Scientific Research and Graduate Studies, and the Faculty of Engineering. Their support is greatly appreciated.

Conflict of interest

The authors declare that there are no conflicts of interest regarding the publication of this manuscript.

Author Contribution Statement

Assim Hameed Yousif Al Daraje: designed and implemented the device. He supervised the experiments and the findings of this work.

Afrah Turki Awad: proposed the research problem and wrote up the manuscript.

Mohamed Gogazeh: co-supervised the experimental tests. Hanan Afeef Mohammad Khamees: ran the experimental tests.

References

1. Liu, K., 2021. *Heat transfer characteristics of triple-stage impingement designs and their application for industrial gas turbine combustor liner cooling. International*. Journal of Heat and Mass Transfer, Vol. 172, pp.121174.

   https://doi.org/10.1016/j.ijheatmasstransfer.2021.121174

2. Son, C., Dailey, G., Ireland, P. and Gillespie, D., 2005, January. *An investigation of the application of roughness elements to enhance heat transfer in an impingement cooling system*. In Turbo Expo: Power for Land, Sea, and Air, Vol. 47268, pp. 465-479.

   https://doi.org/10.1115/GT2005-68504

3. Tawfek A. A., 2002, *Heat transfer studies of the oblique impingement of round jets upon a curved surface*, International Journal of Heat Mass Transfer, Vol. 38, pp. 467–475. DOI: https://doi.org/10.1007/s002310100221

4. Zuckerman N. and Lior N., 2005, *Impingement heat transfer: correlations and numerical modeling*, Journal of Heat Transfer, Vol. 127, Issue 5, pp. 544-552. https://doi.org/10.1115/1.1861921

5. San Y.and Lai M., 2001, *Optimum jet-to-jet spacing of heat transfer for staggered arrays of impinging air jets*, International Journal of Heat Mass Transfer, Vol. 44, Issue 21, pp. 3997–4007. https://doi.org/10.1016/S0017-9310(01)00043-6

6. Changmin S., David G., Peter and Geoffrey M., 2001, *Heat transfer and flow characteristics of an engine representative impingement cooling system*, International Gas Turbine Institute, ASME Journal of Turbomachinery, Vol. 123. Issue 1, pp. 154-160

   https://doi.org/10.1115/1.1328087

7. Brevet P., Dejeu C., Dorignac E. E., Jolly M., and Vullierme J. J., 2002, *Heat transfer to a row of impinging jets in consideration of optimization*, International Journal of Heat and Mass Transfer. Vol. 45, Issue 20, pp. 4191-4200

   https://doi.org/10.1016/S0017-9310(02)00128-X

8. Lamyaa A. E., and Deborah A. K., 2005, *Experimental investigation of local heat transfer distribution on smooth and roughened surfaces under an array of angled impinging*, ASME Journal of turbomachinery, Vol. 127. Issue 3, pp. 532-544

   https://doi.org/10.1115/1.1861918

9. Uysal U., Chyu M. K., and Cunha F. J., 2006, *Heat transfer on the internal surface*

of a duct subjected to impingement of a jet array with varying hole size and spacing, ASME Journal of Turbomachinary, Vol. 128, Issue 1, pp. 158-165

https://doi.org/10.1115/1.2101859

10. Yamane1 Y., Ichikawa1 Y., Yamamoto M. and Honami S., 2012, *Effect of injection parameters on jet array impingement heat transfer*, International Journal of Gas Turbine, Propulsion, and Power Systems, Vol. 4, Issue 1. pp. 27-34

    https://doi.org/10.38036/jgpp.4.1_27

11. Shariatmadar, H., Mousavian, S., Sadoughi, M. and Ashjaee, M., 2016. *Experimental and numerical study on heat transfer characteristics of various geometrical arrangement of impinging jet arrays*. International Journal of Thermal Sciences, Vol. 102, pp.26-38.

    https://doi.org/10.1016/j.ijthermalsci.2015.11.007

12. Flávia V. Barbosa, João P. V. Silva, Pedro E. A. Ribeiro, Senhorinha F. C. F. Teixeira, Delfim F. Soares,Duarte Santos, Maria F. Cerqueira and José C. F. Teixeira, 2018. *An Experimental Setup for Multiple Air Jet Impingement Over a Surface*, ASME 2018 International Mechanical Engineering Congress and Exposition, Volume 8B: Heat Transfer and Thermal Engineering Pittsburgh, Pennsylvania, USA, November 9–15, 2018 https://doi.org/10.1115/IMECE2018-87995

13. Wae-hayee M., Tekasakul P., and Nuntadusit C., 2013, *Influence of nozzle arrangement on flow and heat transfer characteristics of arrays of circular impinging jets*, Journal of Science Technology. Vol. 35, Issue 2, pp. 203-21. https://thaiscience.info/Journals/Article/SONG/10891020.pdf

14. Wae-hayee M., Tekasakul P., Eiamsa S. and Nuntadusit C., 2014. *Effect of cross-flow velocity on flow and heat transfer characteristics of impinging jet with low jet-to-plate distance*, Journal of Mechanical Science and Technology July, Vol. 28, Issue 7, pp 2909–2917. DOI: https://doi.org/10.1007/s12206-014-0534-3

15. Yousif A., Al-Dabagh A. and Aun S., 2016. *Experimental study of heat transfer parameters of impingement heating system represented by conductive target plate of resistive film*, Engineering and Technology Journal, Vol. 34 part (A), Issue 8, pp. 1588-1604 https://www.iasj.net/iasj/download/cbf1ebd5e25a73bc

16. Schroder A., Ou S. and Ghia U., 2016. *Experimental study of an impingement cooling jet array using an infrared thermography technique*, Journal of thermophysics and heat transfer, Vol. 26, Issue 4, pp. 590-597

    https://doi.org/10.2514/1.T3812

17. Keenan M., Amano R. S. and Ou S., 2013. *Study of an impingement cooling jet array for turbine blade cooling with single and double exit cases*, ASME Turbo Expo 2013: Turbine Technical Conference and Exposition, Volume 3A: Heat Transfer, San Antonio, Paper No. GT2013-94116, Texas, USA, June 3–7 https://doi.org/10.1115/GT2013-94116

18. Yang, X., Wu, H. and Feng, Z., 2022. *Jet impingement heat transfer characteristics with variable extended jet holes under strong crossflow conditions*. Aerospace,

Vol. 9, Issue 1, p.44. https://doi.org/10.3390/aerospace9010044

19. Shah, S., 2022. *A Numerical Study of Heat Transfer From an Array of Jets Impinging on a Flat Moving Surface*. Journal of Heat Transfer, Vol. 144, Issue 4, p.042302.

https://doi.org/10.1115/1.4053451

20. Zhou, J., Tian, J., Lv, H. and Dong, H., 2022. *Numerical investigation on flow and heat transfer characteristics of single row jet impingement cooling with varying jet diameter*. International Journal of Thermal Sciences, Vol. 179, p.107710.

https://doi.org/10.1016/j.ijthermalsci.2022.107710

21. Abo El–Wafa, A., Attalla, M., Maghrabie, H.M. and Shmroukh, A.N., 2023. *Influence of Impinging Jet Nozzle Movement on Heat Transfer Characteristics of a Flat Plate*. ASME Journal of Heat and Mass Transfer, Vol. 145, Issue 9

https://doi.org/10.1115/1.4062639

22. Tepe, A.Ü., Yetişken, Y., Uysal, Ü. and Arslan, K., 2020. *Experimental and numerical investigation of jet impingement cooling using extended jet holes*. International Journal of Heat and Mass Transfer, Vol. 158, p.119945.

https://doi.org/10.1016/j.ijheatmasstransfer.2020.119945

23. Wang, J., Kong, H., Xu, Y. and Wu, J., 2019. *Experimental investigation of heat transfer and flow characteristics in finned copper foam heat sinks subjected to jet impingement cooling*. Applied Energy, Vol. 241, pp.433-443.

https://doi.org/10.1016/j.apenergy.2019.03.040

24. Bonds, M., Iyer, G. and Ekkad, S.V., 2023. *Effects Of Variable Pressure Outlets For Array Jet Impingement Cooling With A Bidirectional Exit Air Scheme*. ASME Journal of Heat and Mass Transfer, pp.1-26.

https://doi.org/10.1115/1.4063106

25. Taha, D.Y., Khudhur, D.S. and Nassir, L.M., 2022. *The behavior of heat sink-impingement cooling with flat plate and arced fins models.* Journal of Engineering and Sustainable Development, Vol. 26, Issue 1, pp.1-14.

https://doi.org/10.31272/jeasd.26.1.1

26. Yi, L., Yang, S. and Pan, M., 2022. *Experimental investigation and parameter analysis of micro-jet impingement heat sink for improved heat transfer performance*. Chemical Engineering and Processing-Process Intensification, Vol. 174, p.108867.

https://doi.org/10.1016/j.cep.2022.108867

27. Plant, R.D., Friedman, J. and Saghir, M.Z., 2023. *A Review of Jet Impingement Cooling.* International Journal of Thermofluids, Vol. 17, p.100312.

https://doi.org/10.1016/j.ijft.2023.100312

28. Al Daraje A. H. Y., 2019. *Establishing a Low and Variable Voltage Power Supply System with Digital Control*, SSD conference, IEEE, (SCI.2-2) 1570498603, March 21-24, 2019, Istanbul, Turkey.

https://doi.org/10.1109/SSD.2019.8893201

29. Ou S., and Rivir R., 2006, *Shaped-Hole Film Cooling With Pulsed Secondary Flow*, ASME Paper, No. GT2006-90272, International Gas Turbine Institute, 2006. https://doi.org/10.1115/GT2006-90272

30. Bejan A. A., 2004, Convection Heat Transfer, Wiley, pp. 198.

31. Klin S. J. and McClintock F. A., 1953, Describing uncertainties in single sample *experimental*, Mechanical Engineering, Vol. 75, pp. 3-ns. https://cir.nii.ac.jp/crid/1572261549103675008

32. Sundén, B., 2017. *Advanced heat transfer topics in complex duct flows*. In Advances in Heat Transfer, Vol. 49, pp. 37-89. Elsevier.

https://doi.org/10.1016/bs.aiht.2017.09.001